Article

Not peer-reviewed version

GIS/Remote-Sensing-Based Assessment of Vegetation Health Related to Agroecological Practices in the Southeast of Togo

Folega Fousseni *, Atakpama Wouyo, Pereki Hodabalo, Badabate Diwediga, Ivan Pontin Novotny, Anne Dray, Claude Gracia, Wala Kperkouma, Batawila Komlan, Akpagana Koffi

Posted Date: 21 June 2023

doi: 10.20944/preprints202306.1465.v1

Keywords: biomass; ecophysiology; GIS remote sensing; agroecology; Togo

Article

GIS/Remote-Sensing-Based Assessment of Vegetation Health Related to Agroecological Practices in the Southeast of Togo

Folega Fousseni [1,*], Atakpama Wouyo [1], Pereki Hodabalo [1], Diwediga Badabaté [1], Ivan Pontin Novotny [2], Anne Dray [2], Garcia Claude [2], Wala Kperkouma [1], Batawila Komlan [1] and Akpagana Kofi [1]

[1] 1Laboratory of Botany and Plant Ecology, Department of Botany, Faculty of Sciences, University of Lomé, Togo, 01 BP 1515, Lomé-Togo
[2] Groupe de Foresterie pour le développement / ITES-Ecosystem Management / ETH de Zurich (Suisse)
* Correspondence: ffolegamez@gmail.com; Tel.: 00228 97601665

Abstract: In the context of climate change, the need for stakeholders to contribute to achieving SDG2 is no longer in doubt especially in sub-Saharan Africa. In this study of the landscape within 10 km of the Donomadé model farm, southeastern Togo, we sought to assess vegetation health in ecosystems and agrosystems, including their capacity to produce biomass for agroecological practices. Sentinel-2 sensor data from 2015, 2017, 2020, and 2022 were preprocessed and used to calculate normalized vegetation fire ratio index (NBR), vegetation fire severity index (dNBR), and CASA-SEBAL models. From these different analyses, it was found that vegetation stress increased across the landscape depending on the year of the time series. We estimated that 9952.215 ha, 10,397.43 ha, and 9854.90 ha were highly stressed in 2015, 2017, and 2020, respectively. Analysis of the level of interannual severity revealed the existence of highly photosynthetic areas which had experienced stress. These areas, which were likely to have been subjected to agricultural practices, were estimated to be 8704.871 ha (dNBR2017–2015), 8253.17 ha (dNBR2020–2017), and 7513.93 ha (dNBR2022–2020). In 2022, the total available biomass estimated by remote sensing for was 3,741,715 ± 119.26 kgC/ha/y. The annual average was 3401.55 ± 119.26 kgC/ha/y. In contrast, the total area of healthy vegetation was estimated to be 4594.43 ha, 4301.30 ha, and 4320.85 ha, in 2015, 2017, and 2022, respectively. The acceptance threshold of the net primary productivity (NPP) of the study area was 96%. The coefficient of skewness (0.81 ± 0.073) indicated a mosaic landscape. Productive and functional ecosystem components were present, but these were highly dispersed. These findings suggest a great opportunity to promote agroecological practices. Mulching may be an excellent technique for enhancing overall ecosystem services as targeted by the SDGs, by means of reconversion of plant biomass consumed by vegetation fires or slash-and-burn agricultural practices.

Keywords: biomass; ecophysiology; GIS remote sensing; agroecology; Togo

1. Introduction

As a multifunctional resource, plant biomass has always played a vital role in human life. Today, it is a source of food, energy, and materials for thousands of millions of people. However, ecological sustainability and global food security are also major contemporary concerns [1]. Despite the importance of natural ecosystems in general, and agroecosystems in particular, for poverty reduction and food security, such systems are those most disturbed and threatened by anthropogenic pressures and climate change.

In sub-Saharan Africa, agriculture accounts for about 36% of the gross domestic product and 65% of employment [2]. However, the sector faces many challenges, including a growing demand for food and the environmental impact of conventional agriculture. It is vital that ecological supply and

 doi:10.20944/preprints202306.1465.v1

consumption remain in balance. Agriculture must also be able to meet local survival and development needs [3]. Over the past few decades, modern agricultural practices have often been detrimental to the environment and to human health [4,5]. Rapidly urbanizing populations have profoundly affected land use and land cover, leading to changes in the supply of, and demand for, ecosystem services [3,6]. In response to these changes, many rural communities have adopted agroecological practices to improve the sustainability and resilience of their food-producing systems. Reducing the use of nonorganic fertilizers, promoting biodiversity, and improving soil quality are some of methods used to achieve the goal of scaling up, and to promote agroecological practices.

In Togo, agricultural practices have significant environmental and social impacts [7]. Farmers face the challenges of climate change, biodiversity loss, and food insecurity. Against this backdrop, more attention needs to be paid to ecosystem stability by implementing agroecological restoration projects to achieve sustainable development goals [8].

In southeastern Togo, various agricultural practices have been experimentally introduced, promoted, and implemented in the farming environment. Among these, mulching has recently received particular attention because of its many advantages [9]. These agricultural practices aim to protect and restore soil health, biodiversity, and agricultural ecosystems [10]. They also ensure sufficient food production while minimizing negative environmental impacts. Understanding vegetation health and biomass availability in agricultural areas is essential for assessing the effectiveness of these agroecological practices.

A promising method for assessing vegetation health and biomass availability is the use of geographic information systems and remote sensing. Indeed, for the sustainable management of green biomass, including residues, the use of satellite-based remote sensing products to investigate the effects of post-fire rehabilitation treatments on vegetation appears to represent a significant opportunity. Among the form of spectral-index-based remote sensing commonly used for biomass estimation is the normalized difference vegetation index (NDVI) [11,12].

A considerable number of remote sensing studies have used the NDVI algorithm [13] to assess burn severity [14,15], and the normalized burn ratio (NBR) has been adopted as the standard spectral index for estimating fire/burn severity [16,17]. As mentioned above, vegetation indices based on remote sensing data can effectively reflect canopy chlorophyll ratios. Hence, they are often used to calculate FPAR (photosynthetically active radiation). Other green biomass assessment models take different environmental factors into account.

In Togo, the low productivity of crops increases the vulnerability of local populations [18]. Despite a small population size and the presence of rivers and wetlands, socioeconomic and ecological factors mean that the country faces significant exposure to climate change [19]. The Model Farm of Donomadé (FeMoDo) initiative was established in 2015 near the National Park of South Togodo to mitigate the long-lasting effect of vulnerability in the Donomadé ecovillage [20]. The main objective of FeMoDo is to promote agroecological best practices among rural communities to add value to food crops. The low-cost and appropriate agroecological practices best suited to the context of Donomadé are agroforestry combined with mulching. However, within a radius of 200 m from the model farm, grasslands become increasingly scarce [21]. It is therefore crucial to better understand the impact of agroecological practices on the health of agroecosystems. Promoting agroecological best practices will help guide natural resource management decisions in Togo. In this study, we assess vegetation health and biomass availability in agroecological production systems in Togo.

2. Materials and Methods

2.1. Study Area and Scope

The study area was located in the southeast of Togo, in West Africa (Figure 1). The focal point of the study was the ecovillage of Donomadé. It is located about 130 km from Lomé, the capital of Togo. The geomorphology of the Donomadé zone consists of a peneplain covered by infertile soils degraded by intensive agriculture and slash-and-burn cultivation [22]. The ecovillage is included in the transboundary Mono River biosphere [23,24]. The climate is subequatorial Guinean with 1000

Preprints (www.preprints.org) | NOT PEER-REVIEWED | Posted: 21 June 2023 doi:10.20944/preprints202306.1465.v1

mm.y^{-1} annual average rainfall and an average temperature of 27.6 °C [25]. The main crops grown are maize, cassava, and groundnut. New agroecological practices have spread from the Donomadé model farm (FeMoDo) to the surrounding area in recent years.

A zoning approach was adopted to assess the availability of plant materials and their accessibility for mulching purposes. A series of concentric buffer zones with radii of 200 m, 2 km, 5 km, and 10 km were designed, with the model farm at the center, using the geoprocessing tools in QGIS software (Figure 1).

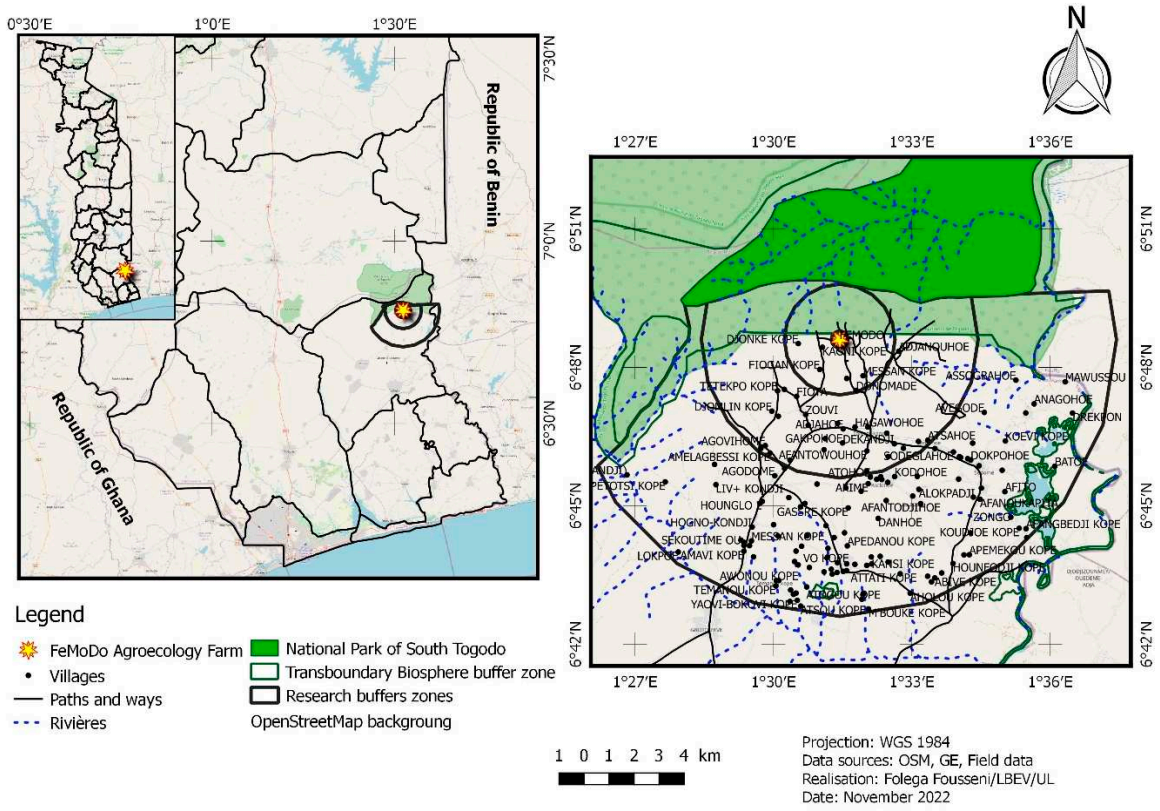

Figure 1. Study area.

2.2. Data Sources and Preprocessing

Sentinel-2 sensor images were acquired free of charge from ESA [26] as part of the Copernicus program [27]. Images from the Sentinel-2B satellite are used in this paper. The characteristics of the Sentinel-2B raw-image time series are shown in Table 1.

Table 1. Nature of Sentinel-2B images [28].

Sentinel-2B	Center wavelength (nm)	Spatial resolution (m)
Band 1—Coastal aerosol	442.2	60
Band 2—Blue	492.1	10
Band 3—Green	559.0	10
Band 4—Red	664.9	10
Band 5—Vegetation red edge	703.8	20
Band 6—Vegetation red edge	739.1	20
Band 7—Vegetation red edge	779.7	20
Band 8—NIR	832.9	10
Band 8A—Narrow NIR	864.0	20
Band 9—Water vapor	943.2	60
Band 10—SWIR—Cirrus	1376.9	60

 doi:10.20944/preprints202306.1465.v1

Band 11—SWIR	1610.4	20
Band 12—SWIR	2185.7	20

The Sentinel-2B datasets acquired for this study consisted of images from December 2015, 2017, 2020, and 2022. They covered the southeast of Togo, extending into the southwest of neighboring Benin. After extracting the layers and stacking the spectral bands, atmospheric correction was performed using the Dark Object Subtraction (DOS1) method [29]. This method is an add-on to QGIS software [30]. The DOS function is one of the most commonly used atmospheric correction methods. It enables use of the stretch function by converting raw or TOA (top-of-atmosphere) digital numbers into reflectance values [31,32]. The QGIS 2.18 masking feature was used to extract the survey area from the four enhanced scenes. The National Institute of Statistics (INSEED/Togo) database was used to collect secondary data on population, climate, and agriculture [33]. Downscaled data from socioeconomic field surveys were also used to interpret the processed images.

2.3. Vegetation Ecophysiology Assessment Using the Normalized Burn Ratio (NBR) Model

The Normalized Burn Ratio (NBR) is a standard vegetation index widely used to highlight burned areas in areas where fire often occurs. The NBR is considered the standard for fire severity assessment [34]. The combination of near-infrared (NIR) and mid-infrared (MIR) reflectance allow the NBR index to be considered as an operational tool [34,35] for assessing the vigor and moisture of vegetation on a national scale. However, the NBR formula is too similar to that of NDVI [17]. To take advantage of the magnitude of the spectral difference provided by remote sensing data, the NBR equation uses the ratio between NIR (near-infrared) and SWIR (shortwave-infrared) bands.

The NBR formula used in this study combines the use of both NIR (B8A) and SWIR (B12) wavelengths (Table 1), and is defined as:

$$NBR = \frac{NIR(B8A) - SWIR(B12)}{NIR(B8A) + SWIR(B12)} \quad (1)$$

A high NBR value generally indicates healthy vegetation conditions. A low value suggests bare ground and/or recently burned areas. Values close to zero indicate unburnt areas [36].

The burn severity rating (dNBR) was calculated from the NBR products of the current study to express the dynamics of vegetation health. The difference between the NBRs obtained from the images for years one and two was used to calculate the delta NBR. This could then be used to estimate the burn severity rating. The dNBR formula is shown below:

$$dNBR\ or\ \Delta NBR = PrefireNBR - PostfireNBR \quad (2)$$

dNBR values vary widely from case to case, so interpretation in specific cases should also be carried out by ELD assessment so that the best results may be obtained. A higher value of *dNBR* indicates more severe damage, but areas with negative *dNBR* values may be experiencing regrowth. The interpretation of fire severity (Table 2) promoted by the United States Geological Survey (USGS) [35] was adopted for the purposes of this study.

Preprints (www.preprints.org) | NOT PEER-REVIEWED | Posted: 21 June 2023 doi:10.20944/preprints202306.1465.v1

Table 2. Burn severity levels obtained by calculating *dNBR*, proposed by USGS [35].

Severity Level	dNBR Range (scaled by 10^3)	dNBR Range (not scaled)
Enhanced Regrowth, high (post-fire)	- 500 to - 251	- 0.500 to - 0.251
Enhanced Regrowth, low (post-fire)	- 250 to - 101	- 0.250 to - 0.101
Unburned	- 100 to + 99	- 0.100 to + 0.99
Low Severity	+ 100 to + 269	+ 0.100 to + 0.269
Moderate-low- Severity	+ 270 to + 439	+ 0.270 to + 0.439
Moderate-high- Severity	+ 440 to + 659	+ 0.440 to + 0.659
High- Severity	+ 660 to + 1300	+ 0.660 to + 1.300

2.4. Spatial Estimation of Vegetation Biomass Using the Net Primary Production (NPP) Model

Remote sensing provides spatially and temporally continuous data for quantifying and monitoring vegetation productivity [16]. Three approaches exist for estimating primary vegetation productivity. The most widely used technique using remote sensing data to estimate NPP is the light use efficiency (LUE) model [37,38]. LUE models estimate vegetation primary productivity by multiplying the remotely sensed fraction of incident photosynthetically active radiation (PAR) absorbed by vegetation (*fAPAR*) by an energy-to-biomass conversion factor, typically referred to as the LUE coefficient.

The NDVI, SR, and NPP-based radiation use efficiency models [39,40] were used to assess the living organic matter available in the landscape in 2022 [3]. The CASA (Carnegie–Ames–Stanford approach) and SEBAL (Surface Energy Balance Algorithm for Land) algorithms [41] were used for model evaluation. NDVI and SR were applied to estimate the fraction of the incident photosynthetically active radiation (FPAR) and absorbed incident photosynthetically active radiation (APAR). This allowed the estimation of the NPP [42] as follows:

$$NPP\ (x,t) = \ APAR \times LUE \tag{3}$$

$$NPP\ (x,t) = \ FPAR(x,t) \times PAR \times LUE \tag{4}$$

where LUE = light use efficiency factor, x = pixel, and t = time.

FPAR has a linear relationship with NDVI and SR [43,44]. FPAR can be calculated from the NDVI and the SR using the following equations:

$$FPAR(x,t) = \frac{\left(SR(x,t) - SR_{i,min}\right) \times (FPAR_{max} - FPAR_{min})}{(SR_{i,max} - SR_{i,\min})} + FPAR_{min} \tag{5}$$

$$FPAR(x,t) = \frac{\left(NDVI(x,t) - NDVI_{i,min}\right) \times (FPAR_{max} - FPAR_{min})}{(NDVI_{i,max} - NDVI_{i,\min})} + FPAR_{min} \tag{6}$$

($FPAR_{max}$ and $FPAR_{min}$ are assumed to be 0.95 and 0.001, respectively).

Estimates of FPAR from the NDVI are usually higher than the absolute values. This is in contrast to calculations based on SR, which tend to be lower than the absolute values [45]. To reduce the error in estimating FPAR, the averaging of NDVI- and SR-derived results has been suggested [46,47]. The following equation was used for this purpose:

$$FPAR\ (x,t) = \propto FPAR_{NDVI} + (1-\propto)FPAR_{SR} \tag{7}$$

α = 0.5 is the adjustment factor of NDVI and SR [3,13].

For clear-sky conditions and in tropical countries, PAR is commonly set to 0.51 [3,48]. The light use efficiency (LUE) is calculated as follows:

$$LUE = \varepsilon \ \times T1 \times T2 \times W \tag{8}$$

Preprints (www.preprints.org) | NOT PEER-REVIEWED | Posted: 21 June 2023 doi:10.20944/preprints202306.1465.v1

where ε = light use efficiency, T1 and T2 relate to plant growth regulation (acclimation) by temperature, and W = the evaporative fraction, calculated thus:

$$W = 0.5 + (EET/PET) \quad (9)$$

where PET is potential evapotranspiration and EET is the estimated evapotranspiration.

Finally, ε is calculated as follows:

$$\varepsilon = \varepsilon^{\circ} \times T1 \times T2 \times W \quad (10)$$

where ε = globally uniform maximum equal to 2.5 g/MJ, T1 relates to the mean temperature during the month of maximum NDVI, and T2 relates to both the mean temperature during the month of maximum NDVI (July in the study area) and to the mean monthly air temperature [3,49]. For the purposes of this study, T1 refers to the mean temperature of the entire wet season from April to September.

To validate the estimated NPP results, the calculated NPP was compared with the reference NPP data of regions such as MODIS A17 [50]. By such means, 70 random sampling points were generated. Polygons of 1 m square were then designed for each sampling point. The NPP values were then extracted from the estimated and referenced NPP data and used to model the regression [51,52].

The research complete workflow is illustrated by Figure 2.

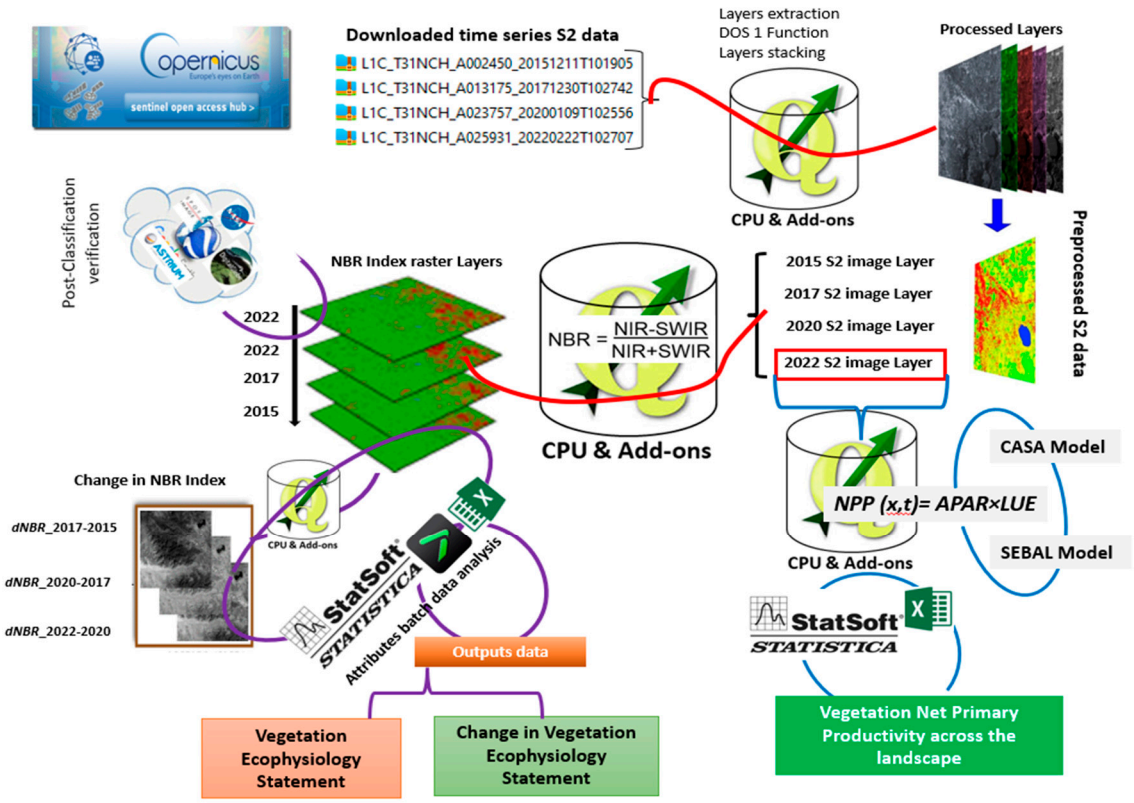

Figure 2. Workflow of the whole approach.

3. Results

3.1. NBR Time Series of Vegetation Health across the Landscape

Statistical averages of NBR (Figure 3) calculated from the Sentinel-2 time series showed a positive increase in the NBR average between 2015 and 2022. For the whole study area, this mean value—which is an ecological indicator—was estimated at 0.034 ± 0.023 in 2015, and 0.104 ± 0.019 in 2022. These results probably imply improved local ecological conditions related to human intervention.

Preprints (www.preprints.org) | NOT PEER-REVIEWED | Posted: 21 June 2023 doi:10.20944/preprints202306.1465.v1

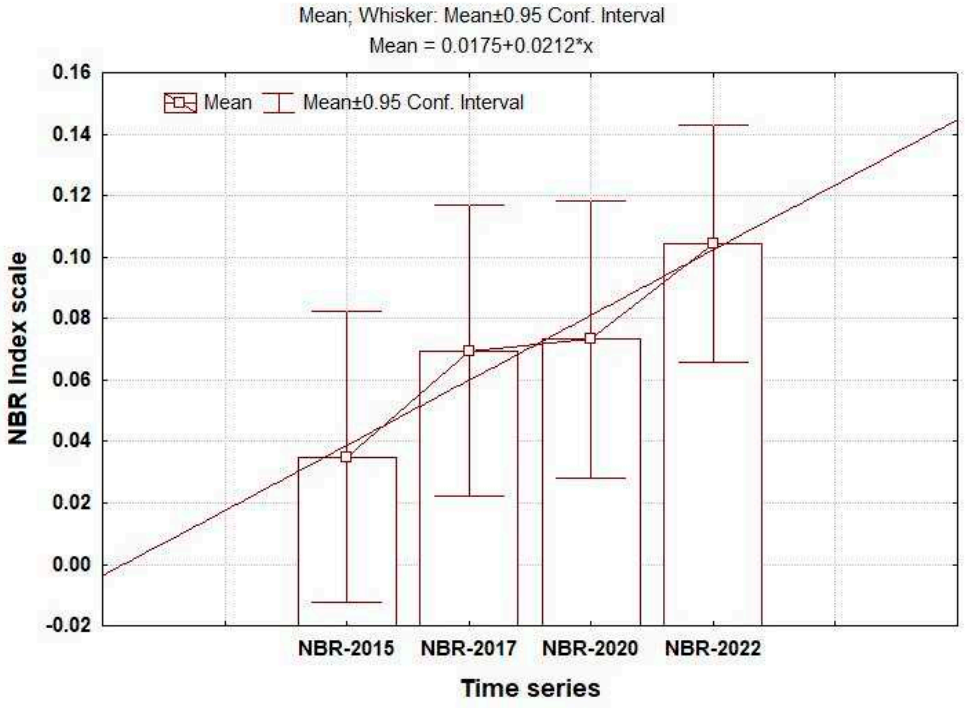

Figure 3. Distribution of normalized burn ratio (NBR) means across the time series.

From a geospatial perspective, four components were distinguished to explain the vegetation health status of the studied landscape. Generally, highly stressed vegetation, represented by the orange color in Figure 4, occupies the southwestern part of the study area in a northeastern direction. This area borders the Southeast of the Togodo National Park and was estimated to comprise 47% (9952.21 ± 0.82 ha) of the total study area in 2015 (Figure 5), increasing slightly to 50% (10,397.43 ± 0.87 ha) in 2017. However, in 2022, the highly stressed vegetation component underwent a significant fragmentation. It was transformed into an area of less-stressed vegetation (Figure 4). In 2022, the spatial fraction of unstressed vegetation was wholly transformed into less-stressed vegetation. This was especially the case in the southern periphery of Togodo South National Park. Thus, the less-stressed fraction increased from 16% (3335.81 ± 0.23 ha) in 2015 to 39% (8177.96 ± 0.34 ha) in 2022.

The vegetation that was unstressed before 2022 was essentially located in the buffer zone of the southern Togodo National Park, and mainly in the transboundary Mono River biosphere (Figure 4). Estimated at 22% (4594.44 ± 0.23 ha) in 2015, this area decreased drastically over the time series.

Preprints (www.preprints.org) | NOT PEER-REVIEWED | Posted: 21 June 2023 doi:10.20944/preprints202306.1465.v1

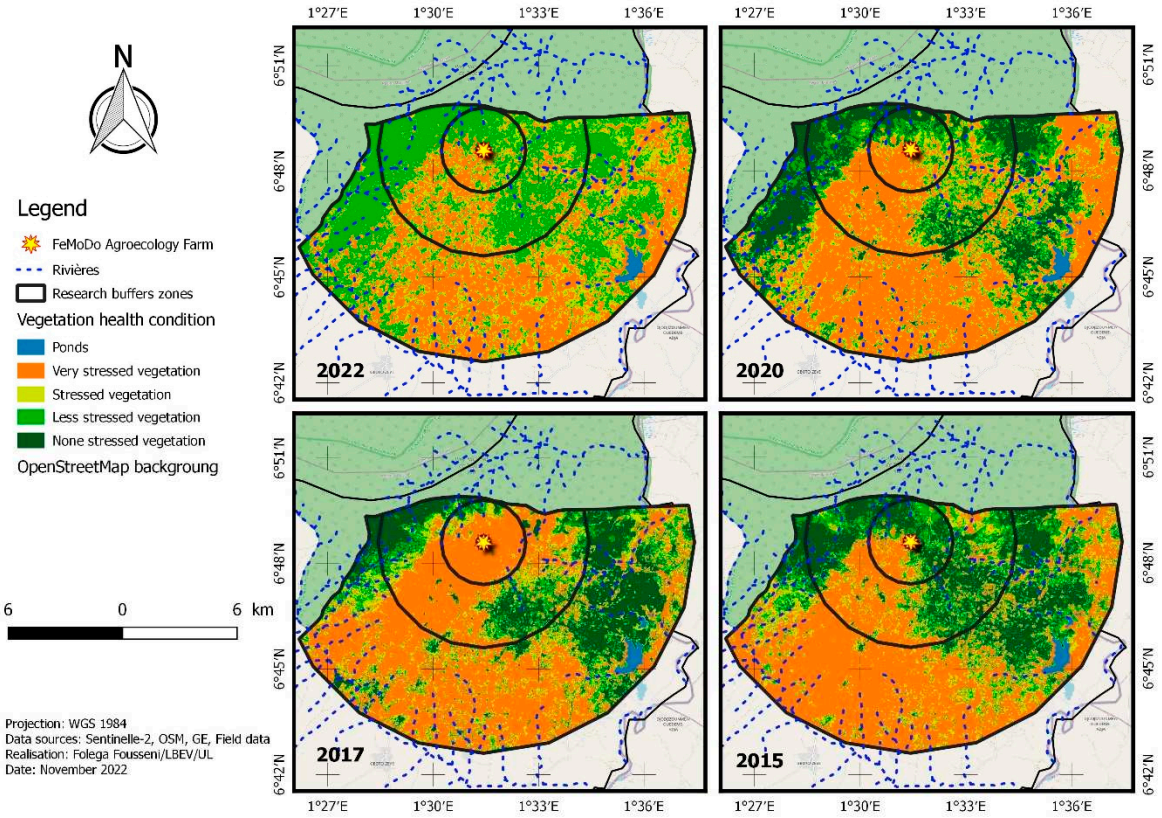

Figure 4. Spatial patterns of vegetation ecophysiological conditions in 2022.

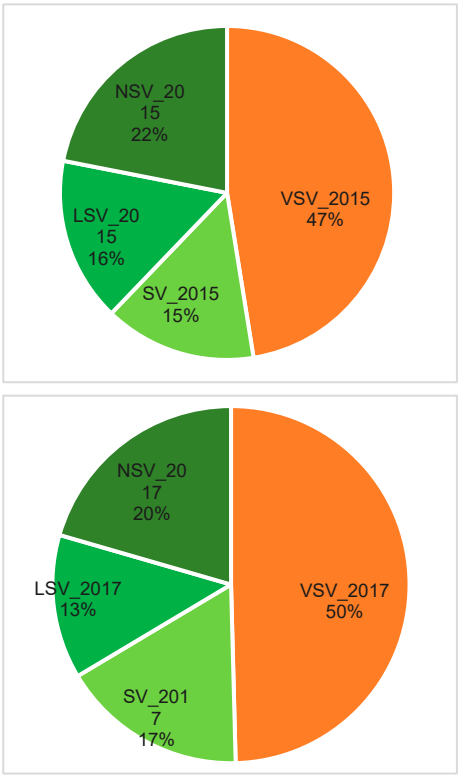

Preprints (www.preprints.org) | NOT PEER-REVIEWED | Posted: 21 June 2023 doi:10.20944/preprints202306.1465.v1

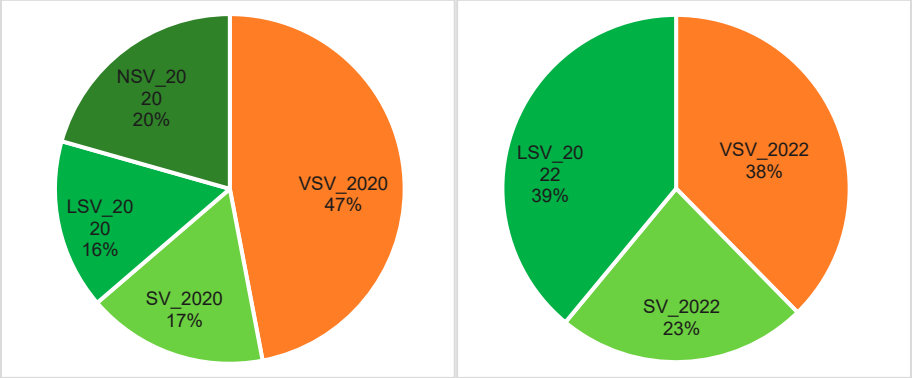

Figure 5. Distribution of normalized burn ratio (NBR) means across the time series.

3.2. Severity of Ecophysiological Conditions of Landscape Vegetation

The analysis of the severity of the physiological conditions governing vegetative growth indicated, in general, a degradation of the vegetation in the studied landscape. This situation is supported by the values of the statistical means of the fire severity index in relation to the vegetation components (Figure 6). The relatively low prevalence of healthy vegetation across the landscape is explained by the average *dNBR* of 0.119 ± 0.033 estimated for 2020–2022. This is further supported by the complete conversion of the less environmentally and anthropogenically disturbed vegetation component to an increasingly disturbed vegetation landscape pattern. The average *dNBR* between 2015 and 2017 was negative (−0.072 ± 0.035), indicating a relatively low level of severity of environmental factors on the whole vegetation component across the studied landscape, compared with the periods 2017–2020 and 2020–2022.

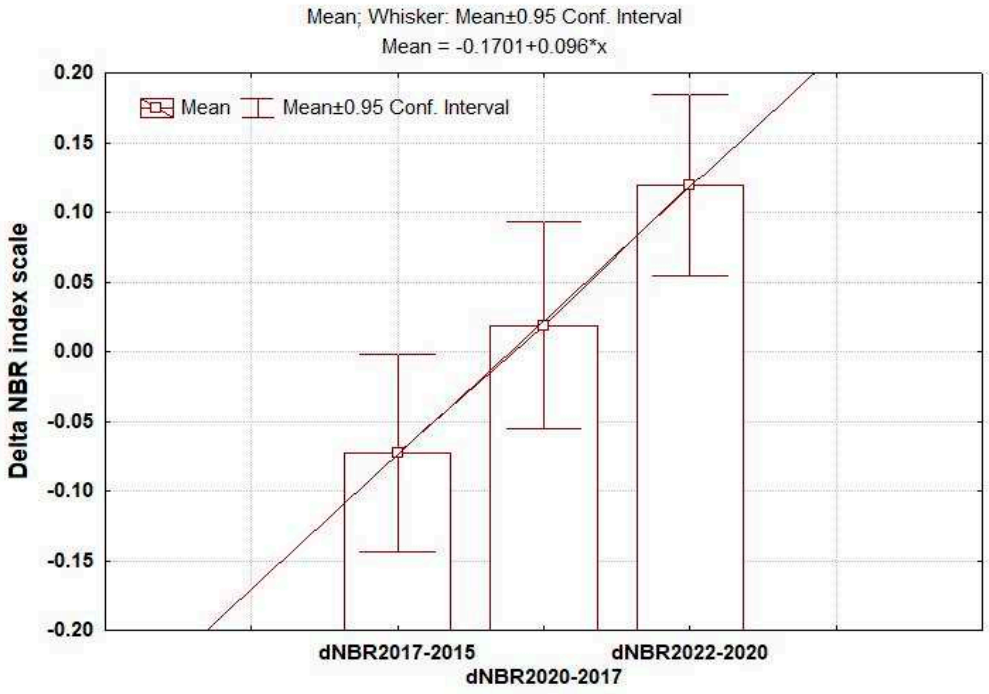

Figure 6. Interannual burn severity mean statistics.

The spatial analysis of the wildfire severity index map products and associated factors showed a stable dispersion of hyper-stressed and highly stressed landscape patches between 2020 and 2022, compared with the periods 2017–2020 and 2015–2017 (Figure 7). During 2015–2017, areas with high wildfire severity and associated factors were located in populated areas of traditional agricultural practices that do not respect agroecological values. During 2017–2020, areas with high wildfire

Preprints (www.preprints.org) | NOT PEER-REVIEWED | Posted: 21 June 2023 doi:10.20944/preprints202306.1465.v1

severity and associated factors were relocated to the western sector, which was less exploited at the time and consists mainly of depressions dominated by grasslands and shrub savannahs.

In the 2017–2015 period (dNBR2017-2015), 40.22% of the vegetation was hyper-stressed, compared with 37.14% for the 2022–2020 period. The area of hyperstressed vegetation was almost zero between 2022 and 2020. The area of highly stressed vegetation was 24.77% in 2017–2015, 24.61 in 2020–2017, and 41.95% in 2022–2020. The area of unstressed vegetation was 6.82% in 2017–2015, 6.77% in 2020 to 2017, and 10.90% in 2022–2020. The highest vegetation regrowth (IRAS) was 5.33% in 2017–2015, 6.44% in 2020–2017, and 9.69% in 2022–2020. In contrast, the lowest vegetation regrowth after stress (FRAS) was 8.20% in 2017–2015, 10.17% in 2020–2017, and 14.27% in 2022–2020 (Figure 8).

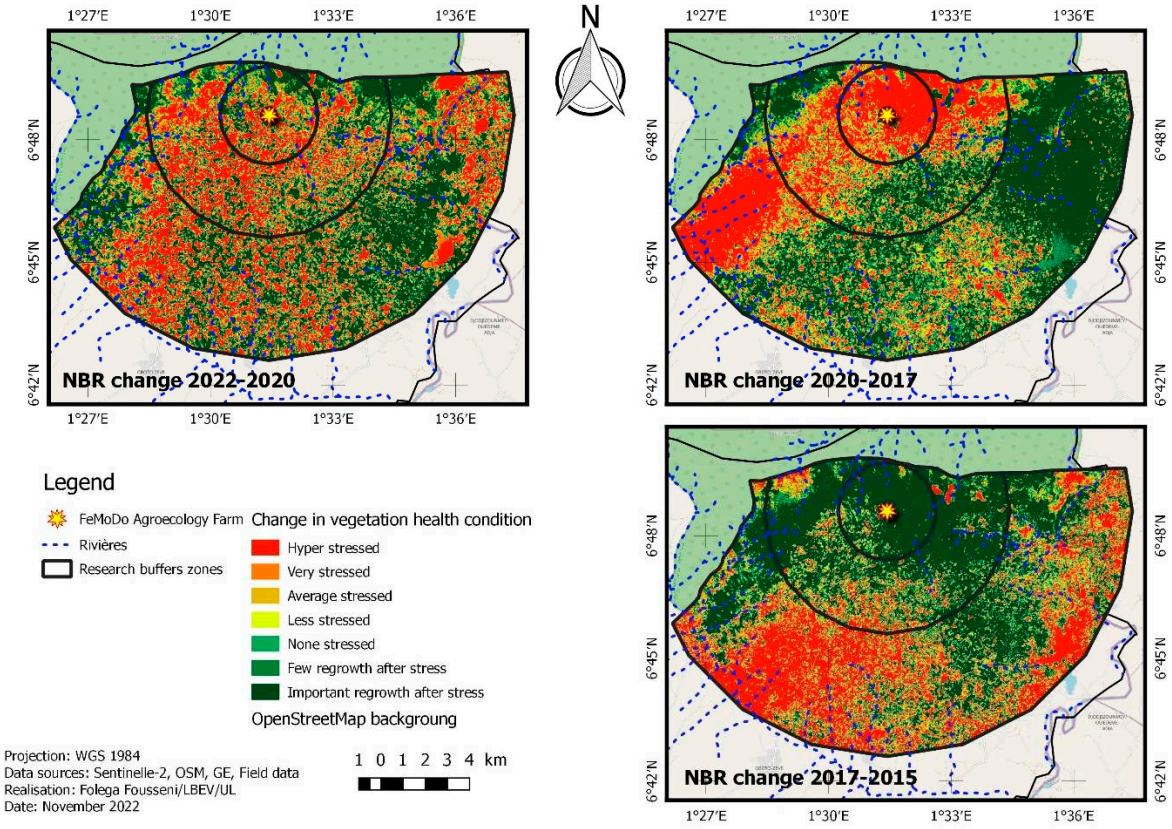

Figure 7. Change in spatial patterns of vegetation ecophysiology.

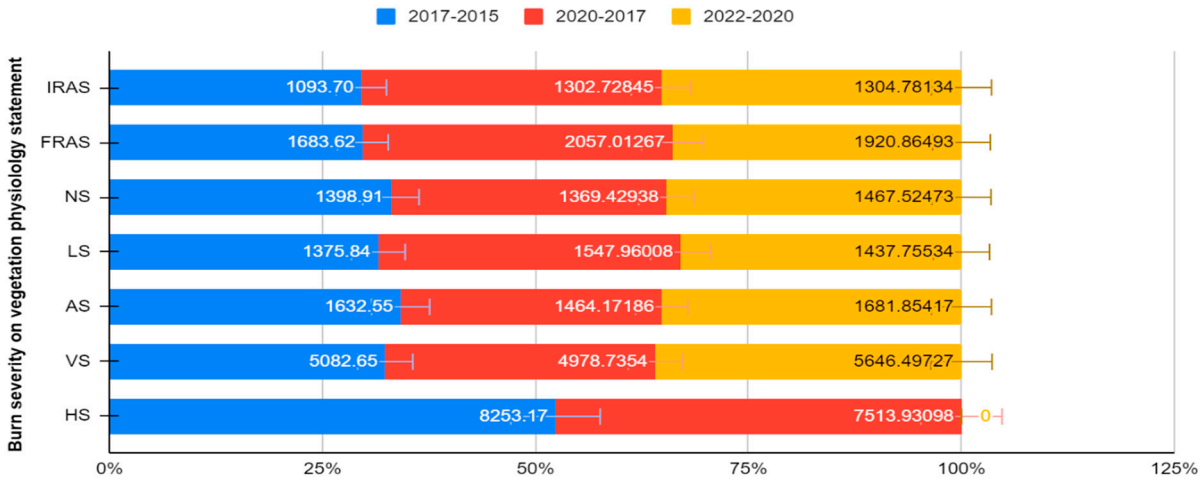

IRAS—Importan t regrowth after stress; FRAS—fewer regrowth after stress; NS—none stressed; LS—less stressed; AS—average stressed; VS—very stressed; HS—hyper-stressed.

Preprints (www.preprints.org) | NOT PEER-REVIEWED | Posted: 21 June 2023 doi:10.20944/preprints202306.1465.v1

Figure 8. Changes in vegetation health condition statistics.

The spatiotemporal distribution of the vegetation *dNBR* showed significant spatial variations across the three periods. In 2020–2017, the vegetation at FeMoDo was quasi-hyper-stressed, while in 2017–2015, there was a very significant regrowth around the farm. Vegetation regrowth is more critical when a longer time period is considered. This explains why the *dNBR* for 2017–2015 is not similar to the other *dNBR* values (Figure 8).

3.3. Global Productivity of Ecosystems' Vegetation across the Landscape

The plant biomass estimated by the CASA-SEBAL model for 2022 correlated highly with the MODA17 reference data. The correlation coefficient R^2 was 0.96. This raised the acceptance threshold of the net primary productivity of the study area to 96% (Figure 9).

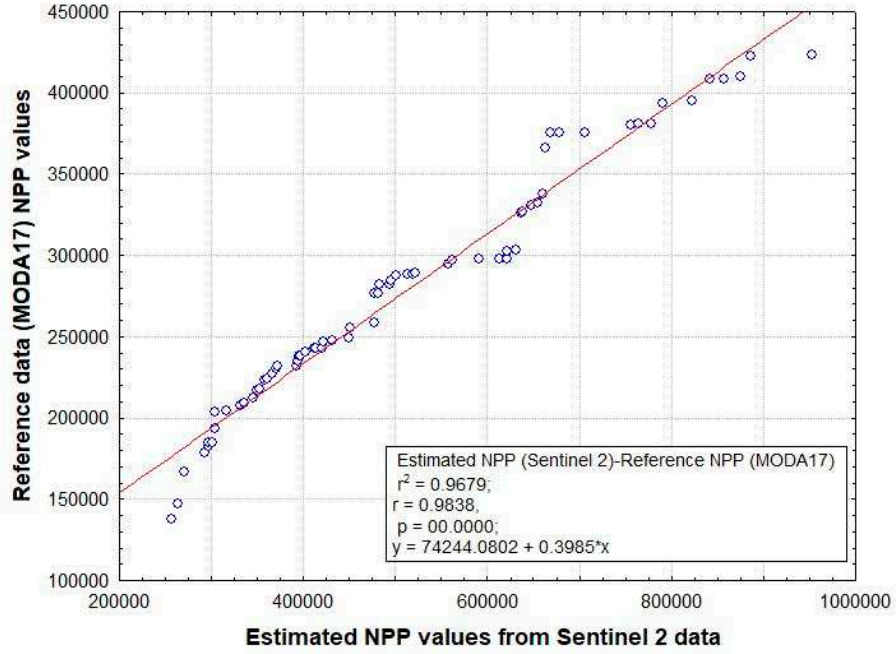

Figure 9. Estimated NPP validation regression curve.

Available biomass or net primary productivity (NPP) ranged from 4.15 to 115.62 kgC/ha in 2022 (Figure 10). The total available biomass estimated was equivalent to 3741715 ± 119.26 kgC/ha/y. The annual average was 3401.55 ± 119.26 kgC/ha/y. The highly positive skewness coefficient (0.81 ± 0.073) indicated a mosaic landscape with productive and functional—but also dispersed—ecosystem components (Figure 10). Thus, permanent wetlands and agrosystems were the areas with high annual biomass productivity (Figure 10). The latter can also be regarded as a reservoir of residual or fresh plant biomass which may be exploited for mulching after production of the various crops. Areas with low productivity or high availability of plant biomass were located in the buffer zone of the protected area; this consists mainly of grass-dominated depressions and shrub savannahs less affected by agricultural practices.

Preprints (www.preprints.org) | NOT PEER-REVIEWED | Posted: 21 June 2023 doi:10.20944/preprints202306.1465.v1

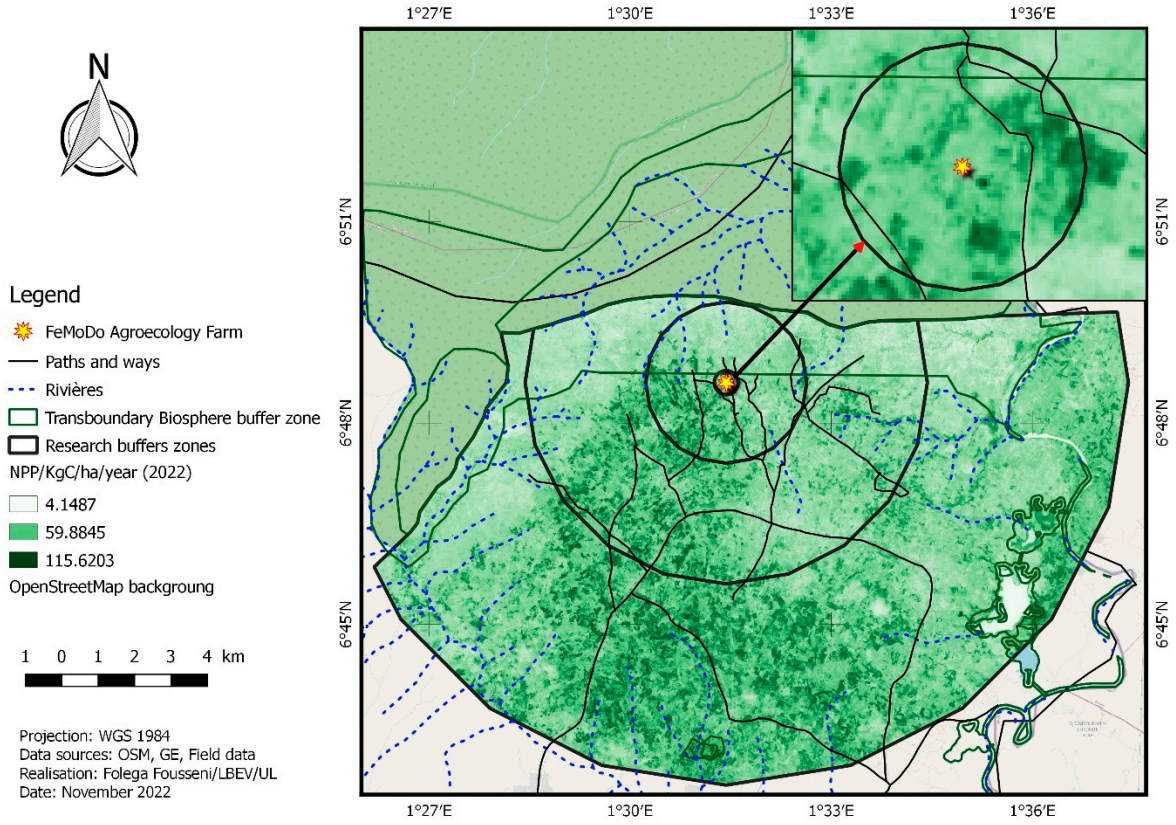

Figure 10. Estimated NPP spatial pattern distribution map.

4. Discussion

Sustainable land management and agroecological approaches are becoming more widely accepted to ensure the sustainability of agricultural systems, whatever their scale of production. Negative impacts on ecosystem services are significantly reduced by integrated management of non- and underutilized phytomass from both forestry and agricultural perspectives [53–55]. In Togo, there is unanimous agreement that landscape approaches can reduce the impact of human-induced drivers [56].

Vegetation health is an essential indicator which measures the effectiveness of agroecological practices on socioecological production factors. Several scientific studies have proposed biomass as an agronomic parameter for crop growth, development, and nutrition [57,58]. In tropical subregions, such as the area in the current study, sustainable management of natural resources for the benefit of the resilience of rural communities has been identified as a vital need. The role of Earth observation data in monitoring vegetation status has never been more critical [59].

The NBR and the dNBR are the most commonly used models for monitoring and assessing ecosystem health. The four landscape patterns of different levels of disturbance to vegetation, mainly caused by wildfire in the study area, show that they are unevenly distributed [44]. The time series product of the NBR shows a regressive trend in terms of the quality of ecosystems and the functioning of agroecosystems. The impact of fire on the landscape was very damaging in 2017, compared with 2015, despite attempts to raise awareness of forest fires led by the National Forest Service, and reinforced by the collaborative actions of local NGOs on the adoption of agroecological best practices since 2015. By 2020, this tendency has been reduced. The fact that 2015 and 2020 were both regarded as drought years in Togo [60] could explain this situation. Another explanation may involve the reappearance of uncontrolled wildfire previously caused by newcomers in the area for cultivation purposes, at least from the perspective of indirect benefits [61] generated by FeMoDo actions.

Changes in vegetation in FeMoDo include abrupt, gradual, and seasonal changes [4,62]. Throughout the time series, the vegetation component of FeMoDo showed an increase in stress levels,

with regular spatial distribution. Similar trends have been observed in African Sahel vegetation dynamics [63]. The results of the present study are also consistent with previous studies of vegetation health using satellite data, which have found vegetation to be sensitive to climatic and agro-demographic stimuli [64]. Increasing productivity was characteristic of some landscape patterns of the study area in the present work, while in other areas this has showed decreasing associations with levels of stress [6]. Such dynamics may occur due to seasonality, the passage of time, climatic conditions, different land use patterns, invasive species, wildfire, and pests [64,65].

The significant correlation (R2 = 0.98) between the calculated NPP and the reference value (MODIS A17) may mean that the finding of the current study is similar to 98% of existing reference NPP data. Current patterns of NPP in the study landscape are the combined result of environmental and land-use changes. Thus, low NPP values in study landscapes could be explained by the fact that they were highly prone to wildfire or had been converted to agricultural land. Other studies have found a similar trend [66,67]. Changes in precipitation and temperature regimes due to climate change can lead to extreme environmental conditions that are detrimental to plant and crop productivity [68]. However, it also appears that the high temperatures resulting from increased evapotranspiration and the arid conditions of this peneplain may strongly affect vegetation growth [69]. The low primary productivity observed mainly at the edge of the buffer zone, especially in protected areas, may be explained by the oldest phytomass components, which are affected annually by wildfire damage. Elsewhere in the landscape, the lower estimated NPPs may be explained by the fact that grasslands and temporary wetlands were generally burned. The increases and decreases in NPP may also have been influenced by the expansion of settlements and population growth, as well as the physico-chemical properties of the soil, as found in previous research [70].

It is mainly the sprawl from FeMoDo towards the periphery that constitutes the permanent active zone due to cropping systems. High values of NPP are observed in patterns consisting of croplands and agroforestry systems under some agroecological practices (around FeMoDo). Whatever the specific patterns of high-productivity processes, the land is continuously exploited for a range of products (maize, cassava groundnut, palms, pineapple, and exotic fruits). This might explain the relatively high rate of NPP in this area. A contribution to green or dead organic matter may also be made by agroecological practices promoted by various NGOs through national and local projects [71].

The different types of mulching practiced in FeMoDo are inspired by ecological principles and social and economic aspects. They show a positive effect on landscape patterns along the positive gradient of crop cover. Phytomass residues from the cultivation process or raw materials from living green plants improve soil quality. This remains a crucial production factor for most of the vulnerable rural communities in Donomadé. A study in Tanzania showed that the plant biomass on agroforestry plots was 70% higher than on conventional annual crop plots [72]. Other studies have confirmed that agroecological practices, such as crop rotation, soil management, and the use of biological pests and disease control methods, can improve vegetation health [73,74].

5. Conclusions

Agroecological practices can bring many benefits to farmers, society, and the environment. In FeMoDo, several agricultural practices make use of mulching. Local conditions and socio-economic factors must be taken into account when deciding on the best method. Based on the observations from the mapping products, between 2015 and 2020, there was a significant level of vegetative stress in the low-geomorphic, grassland-dominated areas that are highly prone to wildfire. Changes in biomass productivity around the FeMoDo vegetation due to climate change and anthropogenic pressures can significantly impact ecosystem processes and biodiversity. This study recommends diversifying forest residues by increasing plant diversity. This alternative could positively impact the quality of plant habitats and the long-term availability of biomass.

Author Contributions: F.F. conceptualized the work, analyzed the data, and wrote the first draft. D.B. W.A. H.P, and I.P.N. contributed to the manuscript editing. All authors have read and agreed to the published version of the manuscript.

Funding: This study was financed by the Swiss National Science Foundation (Grant number IZSTZ0_193032).

Acknowledgments: The study was carried out in collaboration with ITES-Ecosystem Management/ETH of Zurich (Switzerland), the Laboratory of Botany and Plant Ecology (LBEV) of University of Lomé (Togo), and the NGOs "Etoile Verte" and Happy Togo.

Conflicts of Interest: The authors declare that they have no competing interests.

References

1. Zhu, B.; Hashimoto, S.; Cushman, S.A. A two concentric circles model incorporating availability of ecosystem services and affordability of humans to clarify the ecological security concept. *Ecol. Model.* **2023**, *481*, 110343.
2. OCDE, F. L'agriculture en Afrique subsaharienne: Perspectives et enjeux de la décennie à venir. *Perspect. Agric. De L'ocde Et De La FAO* **2016**, *2025*, 63–104.
3. Peng, J.; Wang, X.; Liu, Y.; Zhao, Y.; Xu, Z.; Zhao, M.; Qiu, S.; Wu, J. Urbanization impact on the supply demand budget of ecosystem services: Decoupling analysis. *Ecosyst. Serv.* **2020**, *44*, 101139.
4. Amharref, M.; Aassine, S.; Bernoussi, A.S.; Haddouchi, B.Y. Cartographie de la vulnérabilité à la pollution des eaux souterraines: Application à la plaine du Gharb (Maroc). *Rev. Des Sci. De L'eau* **2007**, *20*, 185–199.
5. Seguin, B.; Soussana, J.-F. Emissions de gaz à effet de serre et changement climatique: Causes et conséquences observées pour l'agriculture et l'élevage. *Le Courr. De L'environnement De L'inra* **2008**, *55*, 79–91.
6. Folega, F.; Datche-Danha, K.E.; Folega, A.A.; Woegan, A.Y.; Wala, K.; Akpagana, K. Diversité des services écosystémiques et utilisation des terres dans le paysage du socle Eburnéen au Togo. *Rev. Nat. Et Technol.* **2022**, *14*, 61–75.
7. Kanda, M.; Djaneye-Boundjou, G.; Wala, K.; Gnandi, K.; Batawila, K.; Sanni, A.; Akpagana, K. Application des pesticides en agriculture maraichère au Togo. *VertigO* **2013**, *13*.
8. Abalo-Esso, M.; Agossou, G.-T.; Blavet, D.; Hien, E.; Chotte, J.L. Dégradation de la fertilité des sols et de l'environnement dans la Région des Savanes au Nord-Togo : Analyse des perceptions et stratégies d'adaptation indigènes. *Eur. Sci. J. ESJ* **2021**, *17*, 40–65.
9. Anani, C.K.S.; Tounou, A.K.; Agboka, K.; Gnon, T.; Kotor, K.E.S. Analyse des impacts agroenvironnementaux et socioéconomiques des systèmes de culture d'ananas (Ananas comosus L.) au Sud-Togo. *J. Appl. Biosci.* **2020**, *153*, 15807–15820.
10. Gnissien, M.; Coulibaly, K.; Senou, I.; Yameogo, T.J.; Nacro, B.H. Diversité des systèmes de cultures et des modes de gestion des ligneux arborés et arbustifs des parcs agroforestiers en zone nord-soudanienne du Burkina Faso. **2022**, *41*, 81–89.
11. Berger, K.; Hank, T.; Halabuk, A.; Rivera-Caicedo, J.P.; Wocher, M.; Mojses, M.; Gerhátová, K.; Tagliabue, G.; Dolz, M.M.; Venteo, A.B.P. Assessing non-photosynthetic cropland biomass from spaceborne hyperspectral imagery. *Remote Sens.* **2021**, *13*, 4711.
12. Tigges, J.; Lakes, T. High resolution remote sensing for reducing uncertainties in urban forest carbon offset life cycle assessments. *Carbon Balance Manag.* **2017**, *12*, 17.
13. Jiang, Z.; Huete, A.R.; Didan, K.; Miura, T. Development of a two-band enhanced vegetation index without a blue band. *Remote Sens. Environ.* **2008**, *112*, 3833–3845.
14. Riva, M.J.; Daliakopoulos, I.N.; Eckert, S.; Hodel, E.; Liniger, H. Assessment of land degradation in Mediterranean forests and grazing lands using a landscape unit approach and the normalized difference vegetation index. *Appl. Geogr.* **2017**, *86*, 8–21.
15. Evangelides, C.; Nobajas, A. Red-Edge Normalised Difference Vegetation Index (NDVI705) from Sentinel-2 imagery to assess post-fire regeneration. *Remote Sens. Appl. : Soc. Environ.* **2020**, *17*, 100283.
16. Mallinis, G.; Mitsopoulos, I.; Chrysafi, I. Evaluating and comparing Sentinel 2A and Landsat-8 Operational Land Imager (OLI) spectral indices for estimating fire severity in a Mediterranean pine ecosystem of Greece. *GIScience Remote Sens.* **2018**, *55*, 1–18.
17. Cardil, A.; Mola-Yudego, B.; Blázquez-Casado, Á.; González-Olabarria, J.R. Fire and burn severity assessment: Calibration of Relative Differenced Normalized Burn Ratio (RdNBR) with field data. *J. Environ. Manag.* **2019**, *235*, 342–349.
18. Gadédjisso-Tossou, A. Understanding farmers' perceptions of and adaptations to climate change and variability: The case of the Maritime, Plateau and Savannah Regions of Togo. *Agric. Sci.* **2015**, *6*, 1441.

19. Munang, R.; Andrews, J.; Alverson, K.; Mebratu, D. Harnessing ecosystem-based adaptation to address the social dimensions of climate change. *Environ. Sci. Policy Sustain. Dev.* **2014**, *56*, 18–24.
20. Adjanke, A.; Tona, K.; Gbeassor, M. Effects of frequency of feeding on feed intake, growth and survival of Nile Tilapia, Oreochromis niloticus reared in hapas implanted in pond in Togo. *Int. J. Fish. Aquat. Stud.* **2021**, *9*, 350–353.
21. Akodéwou, A.; Oszwald, J.; Gazull, L.; Akpavi, S.; Akpagana, K.; Gond, V.; Saidi, S. Land Use and Land Cover Dynamics Analysis of the Togodo Protected Area and Its Surroundings in Southeastern Togo, West Africa. *Sustainability* **2020**, *12*, 5439. https://doi.org/10.3390/su12135439.
22. Akodéwou, A.; Godron, M. Agricultural land-use increases flo-ral species richness in tropical dry forest and savannah ecosystems in West Africa. *Diversity* **2022**, *14*, 106.
23. Abalo, M.; Badabate, D.; Fousseni, F.; Kpérkouma, W.; Koffi, A. Landscape-based analysis of wetlands patterns in the Ogou River basin in Togo (West Africa). *Environ. Chall.* **2021**, *2*, 100013.
24. Gnansounou, S.C.; Salako, K.V.; Sagoe, A.A.; Mattah, P.A.D.; Aheto, D.W.; Glèlè Kakaï, R. Mangrove ecosystem services, associated threats and implications for wellbeing in the Mono Transboundary Biosphere Reserve (Togo-Benin), West-Africa. *Sustainability* **2022**, *14*, 2438.
25. Sodokin, K.; Nyatefe, V. Cash transfers, climate shocks vulnerability and households' resilience in Togo. *Discov. Sustain.* **2021**, *2*, 3.
26. Hub, C.O.A. The Open Access Hub Provides Complete, Free and Open Access to Sentinel-1, Sentinel-2, Sentinel-3 and Sentinel-5P User Products. **2022**.
27. Directorate Space, S.; Migration, E.C.J.R.C. Copernicus Emergency Management Service. **2017**.
28. Handbook, S.U.; Tools, E. *Sentinel-2 User Handbook*; ESA Standard Document; 2015; pp. 1–64.
29. Song, C.; Woodcock, C.E.; Seto, K.C.; Lenney, M.P.; Macomber, S.A. Classification and change detection using Landsat TM data: When and how to correct atmospheric effects? *Remote Sens. Environ.* **2001**, *75*, 230–244.
30. Plakman, V.; Janssen, T.; Brouwer, N.; Veraverbeke, S. Mapping species at an individual-tree scale in a temperate forest, using sentinel-2 images, airborne laser scanning data, and random forest classification. *Remote Sens.* **2020**, *12*, 3710.
31. Folega, F.; Atakpama, W.; Wala, K.; Mukete, B.; Shozo, S.; Akira, O.; Zhao, X.-h.; Akpagana, K. Land use patterns and tree species diversity in the Volta Geological Unit, Togo. *J. Mt. Sci.* **2019**, *16*, 1869–1882. https://doi.org/10.1007/s11629-018-5154-4.
32. Nazeer, M.; Nichol, J.E. Combining landsat TM/ETM+ and HJ-1 A/B CCD sensors for monitoring coastal water quality in Hong Kong. *IEEE Geosci. Remote Sens. Lett.* **2015**, *12*, 1898–1902.
33. Lamboni, M. *Analyses des Données RGPH4-Novembre 2010 (État Matrimonial et Nupitialité)*; Institut National de la Statistique et des Études Économiques Et Démographiques (INSEED-TOGO): Lomé, Togo, 2016.
34. Storey, E.A.; Lee West, K.R.; Stow, D.A. Utility and optimization of LANDSAT-derived burned area maps for southern California. *Int. J. Remote Sens.* **2021**, *42*, 486–505.
35. Alcaras, E.; Costantino, D.; Guastaferro, F.; Parente, C.; Pepe, M. Normalized Burn Ratio Plus (NBR+): A new index for sentinel-2 imagery. *Remote Sens.* **2022**, *14*, 1727.
36. Bright, B.C.; Hudak, A.T.; Kennedy, R.E.; Braaten, J.D.; Henareh Khalyani, A. Examining post-fire vegetation recovery with Landsat time series analysis in three western North American forest types. *Fire Ecol.* **2019**, *15*, 8.
37. Kumar, M.; Monteith, J. Plants and the daylight spectrum. *Remote Sens. Crop Growth* **1981**, 133–144.
38. Tao, F.; Yokozawa, M.; Zhang, Z.; Xu, Y.; Hayashi, Y. Remote sensing of crop production in China by production efficiency models: Models comparisons, estimates and uncertainties. *Ecol. Model.* **2005**, *183*, 385–396.
39. Zhu, Q.; Zhao, J.; Zhu, Z.; Zhang, H.; Zhang, Z.; Guo, X.; Bi, Y.; Sun, L. Remotely sensed estimation of net primary productivity (NPP) and its spatial and temporal variations in the Greater Khingan Mountain region, China. *Sustainability* **2017**, *9*, 1213.
40. Wang, Y.; Xu, X.; Huang, L.; Yang, G.; Fan, L.; Wei, P.; Chen, G. An improved CASA model for estimating winter wheat yield from remote sensing images. *Remote Sens.* **2019**, *11*, 1088.
41. Bastiaanssen, W.G.; Ali, S. A new crop yield forecasting model based on satellite measurements applied across the Indus Basin, Pakistan. *Agric. Ecosyst. Environ.* **2003**, *94*, 321–340.
42. Zhang, Y.; Xu, M.; Chen, H.; Adams, J. Global pattern of NPP to GPP ratio derived from MODIS data: Effects of ecosystem type, geographical location and climate. *Glob. Ecol. Biogeogr.* **2009**, *18*, 280–290.

43. Los, S.O.; Justice, C.; Tucker, C. A global 1 by 1 NDVI data set for climate studies derived from the GIMMS continental NDVI data. *Int. J. Remote Sens.* **1994**, *15*, 3493–3518.
44. Veloso, G.A. *Produtividade primária bruta e biomassa em pastagem no bioma cerrado: Uma análise a partir dos modelos SEBAL/CASA e MOD17 no estado de Goiás*; Universidade Federal de Goiás: Goiânia, Brazil, 2018.
45. Wang, Y.; Yan, G.; Xie, D.; Hu, R.; Zhang, H. Generating long time series of high spatiotemporal resolution FPAR images in the remote sensing trend surface framework. *IEEE Trans. Geosci. Remote Sens.* **2021**, *60*, 4401915.
46. Peng, D.; Zhang, B.; Liu, L.; Fang, H.; Chen, D.; Hu, Y.; Liu, L. Characteristics and drivers of global NDVI-based FPAR from 1982 to 2006. *Glob. Biogeochem. Cycles* **2012**, *26*, GB3015. https://doi.org/10.1029/2011GB004060.
47. Zhu, M.; Zhang, J.; Zhu, L. Article title variations in growing season NDVI and its sensitivity to climate change responses to green development in mountainous areas. *Front. Environ. Sci.* **2021**, *9*, 678450.
48. Jiang, S.; Huang, Y.; Zhao, L.; Cui, N.; Wang, Y.; Hu, X.; Zheng, S.; Zou, Q.; Feng, Y.; Guo, L. Effects of clouds and aerosols on ecosystem exchange, water and light use efficiency in a humid region orchard. *Sci. Total Environ.* **2022**, *811*, 152377.
49. Field, C.B.; Behrenfeld, M.J.; Randerson, J.T.; Falkowski, P. Primary production of the biosphere: Integrating terrestrial and oceanic components. *Science* **1998**, *281*, 237–240.
50. Sun, J.; Yue, Y.; Niu, H. Evaluation of NPP using three models compared with MODIS-NPP data over China. *PLoS ONE* **2021**, *16*, e0252149.
51. Xie, X.; Li, A.; Tan, J.; Jin, H.; Nan, X.; Zhang, Z.; Bian, J.; Lei, G. Assessments of gross primary productivity estimations with satellite data-driven models using eddy covariance observation sites over the northern hemisphere. *Agric. For. Meteorol.* **2020**, *280*, 107771. https://doi.org/10.1016/j.agrformet.2019.107771.
52. de Leeuw, J.; Rizayeva, A.; Namazov, E.; Bayramov, E.; Marshall, M.T.; Etzold, J.; Neudert, R. Application of the MODIS MOD 17 Net Primary Production product in grassland carrying capacity assessment. *Int. J. Appl. Earth Obs. Geoinf.* **2019**, *78*, 66–76. https://doi.org/10.1016/j.jag.2018.09.014.
53. Monette, M.; Hénault-Ethier, L.; Rony, F.J.; Beaudoin Nadeau, M.; Michel, G. Restauration des paysages forestiers et agroforestiers jumelée à la valorisation des déchets organiques en Haïti pour le développement durable d'une économie verte résiliente aux changements climatiques. *Haiti Perspect.* **2018**, *6*, 33–42.
54. Gazull, L. Les filières agricoles et forestières du Sud à l'heure des bioénergies. *Développement durable et filières tropicales, Versailles, Quae*; Biénabe, E., Lœillet, D., Rival, A., Eds.; 2016; pp. 171–182.
55. Diogo, R.V.; Adedigba, S.; Djedje, M.; Dossa, L.H. Gestion et contribution des résidus de récolte à la réduction du déficit alimentaire des élevages traditionnels de petits ruminants dans la zone soudanienne du Nord Bénin. *Ann. UP Série Sci. Nat. Agron* **2018**, *8*, 1–12.
56. Inda, H.; García-Rodríguez, F.; del Puerto, L.; Stutz, S.; Figueira, R.C.L.; de Lima Ferreira, P.A.; Mazzeo, N. Discriminating between natural and human-induced shifts in a shallow coastal lagoon: A multidisciplinary approach. *Anthropocene* **2016**, *16*, 1–15.
57. Liu, Y.; Feng, H.; Yue, J.; Li, Z.; Yang, G.; Song, X.; Yang, X.; Zhao, Y. Remote-sensing estimation of potato above-ground biomass based on spectral and spatial features extracted from high-definition digital camera images. *Comput. Electron. Agric.* **2022**, *198*, 107089.
58. Lu, N.; Zhou, J.; Han, Z.; Li, D.; Cao, Q.; Yao, X.; Tian, Y.; Zhu, Y.; Cao, W.; Cheng, T. Improved estimation of aboveground biomass in wheat from RGB imagery and point cloud data acquired with a low-cost unmanned aerial vehicle system. *Plant Methods* **2019**, *15*, 17. https://doi.org/10.1186/s13007-019-0402-3.
59. Abdelkarim, A. Monitoring and forecasting of land use/land cover (LULC) in Al-Hassa Oasis, Saudi Arabia based on the integration of the Cellular Automata (CA) and the Cellular Automata-Markov Model (CA-Markov). *Geol. Ecol. Landsc.* **2023**, 1–32.
60. Djan'na, K.H.; Atchonouglo, K.; Adounkpe, J.G.; Diwediga, B.; Lombo, Y.; Kpemoua, K.E.; Agboka, K. Changes In Land Use/Cover And Water Balance Components During 1964–2010 Period In The Mono River Basin, Togo-Benin. *Geogr. Environ. Sustain.* **2023**, *15*, 171–180.
61. Bengston, D.N.; Fan, D.P.; Celarier, D.N. A new approach to monitoring the social environment for natural resource management and policy: The case of US national forest benefits and values. *J. Environ. Manag.* **1999**, *56*, 181–193.
62. Zhu, Z.; Woodcock, C.E. Continuous change detection and classification of land cover using all available Landsat data. *Remote Sens. Environ.* **2014**, *144*, 152–171. https://doi.org/10.1016/j.rse.2014.01.011.

63. Herrmann, S.M.; Anyamba, A.; Tucker, C.J. Recent trends in vegetation dynamics in the African Sahel and their relationship to climate. *Glob. Environ. Change* **2005**, *15*, 394–404.
64. Meneses, B.M. Vegetation recovery patterns in burned areas assessed with landsat 8 OLI imagery and environmental biophysical data. *Fire* **2021**, *4*, 76.
65. Akodéwou, A.; Oszwald, J.; Akpavi, S.; Gazull, L.; Akpagana, K.; Gond, V. Problématique des plantes envahissantes au sud du Togo (Afrique de l'Ouest) : Apport de l'analyse systémique paysagère et de la télédétection. *Biotech. Agron. Soc* **2019**, *23*, hal-02288188.
66. Tian, Z.; Qin, T.; Wang, H.; Li, Y.; Yan, S.; Hou, J.; Li, C.; Abebe, S. Delayed response of net primary productivity with climate change in the Yiluo River basin. *Front. Earth Sci.* **2023**, *10*, 1017819. https://doi.org/10.3389/feart.2022.1017819.
67. Ma, B.; Jing, J.; Liu, B.; Xu, Y.; Dou, S.; He, H. Spatiotemporal variation of net primary productivity influenced by climatic variables in the karst area of China. *Geocarto Int.* **2022**, 1–19. https://doi.org/10.1080/10106049.2022.2129845.
68. Houot, S.; Pons, M.-N.; Pradel, M.; Tibi, A. *Recyclage de déchets organiques en agriculture: Effets Agronomiques et Environnementaux de leur Épandage*; Editions Quae: Montpellier, France, 2016.
69. Cheng, Q.; Gao, L.; Zhong, F.; Zuo, X.; Ma, M. Spatiotemporal variations of drought in the Yunnan-Guizhou Plateau, southwest China, during 1960–2013 and their association with large-scale circulations and historical records. *Ecol. Indic.* **2020**, *112*, 106041.
70. Hu, X.; Hou, Y.; Li, D.; Hua, T.; Marchi, M.; Urrego, J.; Huang, B.; Cherubini, F. Changes in multiple ecosystem services and their influencing factors in Nordic countries. *Ecol. Indic.* **2023**, *146*, 109847. https://doi.org/10.1016/j.ecolind.2022.109847.
71. Mier y Terán Giménez Cacho, M.; Giraldo, O.F.; Aldasoro, M.; Morales, H.; Ferguson, B.G.; Rosset, P.; Khadse, A.; Campos, C. Bringing agroecology to scale: Key drivers and emblematic cases. *Agroecol. Sustain. Food Syst.* **2018**, *42*, 637–665.
72. Rufino, M.C.; Dury, J.; Tittonell, P.; Van Wijk, M.T.; Herrero, M.; Zingore, S.; Mapfumo, P.; Giller, K.E. Competing use of organic resources, village-level interactions between farm types and climate variability in a communal area of NE Zimbabwe. *Agric. Syst.* **2011**, *104*, 175–190.
73. Renaud, S.; Colin, D. *Les Rotations de Culture: Intérêt en Agriculture Biologique*; Université de Rennes: Rennes, France, 2017.
74. Perrin, B.; Lefevre, A. L'association culturale, un levier pour améliorer santé des plantes, fertilité du sol et production des systèmes de culture maraichers diversifiés? *Innov. Agron.* **2019**, *76*, 51–70.